International Journal of Coal Geology 246 (2021) 103841

Contents lists available at ScienceDirect

International Journal of Coal Geology

journal homepage: www.elsevier.com/locate/coal

Geochemical influences on methanogenic groundwater from a low rank coal seam gas reservoir: Walloon Subgroup, Surat Basin

K.A. Baublys [a,*], H. Hofmann [a], J.S. Esterle [a], D.I. Cendón [b,c], S. Vink [d], S.D. Golding [a]

[a] School of Earth and Environmental Sciences, The University of Queensland, QLD 4072, Australia
[b] Australian Nuclear Science and Technology Organisation, Lucas Heights, NSW 2234, Australia
[c] School of Biological, Earth and Environmental Sciences, UNSW Sydney, Kensington, NSW 2052, Australia
[d] Sustainable Minerals Institute, The University of Queensland, QLD 4072, Australia

ARTICLE INFO

Keywords:
^{36}Cl
^{14}C
^{18}O
Fluid-rock
Coal-bed-methane
Groundwater
Cosmogenic

ABSTRACT

Hydrochemical data responds at a much slower rate to changes in groundwater conditions than does the propagation of hydraulic pressure, and therefore may provide more insight to groundwater flow paths. In low rank coal measures, where gas is biogenic, it is important to understand the fluid-rock and microbial interactions that affect the spatial and temporal distribution of groundwater composition. Pressure data may not reflect true groundwater conditions pre-anthropogenic influence, nor does it provide information on the main drivers of groundwater composition, actual aquifer behaviour or even prove groundwater flow.

This study uses a process-based approach to interpret a combination of tracer (^{36}Cl, ^{14}C, $^{87}Sr/^{86}Sr$, $^{18}O/^{16}O$) and hydrochemical data obtained from coal seam gas production wells to identify the main geochemical processes and thus controls on the groundwater composition in different coal seam producing areas of the Walloon Subgroup, Surat Basin, Australia. This is arguably one of the largest coal seam gas producing regions in the world. Tracer data measured in this study show that the Walloon Subgroup behaves as a stagnant aquitard, as indicated by the almost total loss of cosmogenic tracers over relatively short groundwater flow distances (~15 km), suggestive of very low ground water flow velocities. The range of ^{36}Cl is 9.0 to 23.8 (x 10^{-15}) while the ^{36}Cl values across the Undulla anticline in the eastern edge of the basin, are essentially the same (12.2–14.7) within analytical error. It is argued that these isotopic values represent secular equilibrium for the Walloon Subgroup. Radiometric carbon (^{14}C) levels across all three production areas (Roma, Undulla Nose, Kogan Nose) are also too low (range = 0.12–1.95 pMC) for viable field interpretation largely owing to the long residence time of the groundwater and the local activity of methanogens. Groundwater flow velocity was estimated to be <0.1 m/y, which is significantly less than the 0.7 m/y recently reported for the underlying Hutton Sandstone.

As a result of the low groundwater flow velocities, trends in geochemistry are visible only in production regions proximal to the subcrop. At flow distances greater than 10–15 km from subcrop, several low-temperature interactions (cation exchange, silicate weathering, matrix diffusion and hyperfiltration) start to influence groundwater composition. Shallow subsurface chemical and microbial reactions may initially dominate the geochemical composition of the meteoric groundwater, but this is then overprinted by the actions of sulfate reducers and methanogens, resulting in groundwater with the typical geochemical characteristics similar to other coal bed methane groundwater in basins across the world (low SO_4, Ca, Mg and high HCO_3, Na, Cl). As distance and depth increase further, low temperature fluid-rock interactions then begin to influence the groundwater composition.

This holistic, process-based approach applied to a combination of cosmogenic and stable isotopes, and standard hydrochemical data interpreted against basin lithology has enabled a more comprehensive picture on the behaviour of the groundwater of the Walloon Subgroup and is applicable to the study of other sedimentary basins.

* Corresponding author.
E-mail address: K.Baublys@uq.edu.au (K.A. Baublys).

https://doi.org/10.1016/j.coal.2021.103841
Received 10 March 2021; Received in revised form 6 August 2021; Accepted 8 August 2021
Available online 10 August 2021

1. Introduction

Identification of the fluid-rock and microbial processes (geological and hydrological) is necessary before the spatial and temporal drivers on groundwater composition in sedimentary basins can be defined. In turn, groundwater fluxes, flow directions and recharge can only be fully understood once the main drivers of groundwater composition are explored in depth.

The discovery of unconventional gas reserves known as coal seam gas (CSG) or more specifically coal bed methane (CBM) within sedimentary basins, such as the Black Warrior, Illinois and Powder River basins in the USA, has contributed much to the current understanding of the groundwater and gas evolutionary processes in coal measures. Determination of the origin of the natural gas (thermogenic, biogenic, abiotic) through analysis of the isotopic and molecular composition of the gas was made possible through the development of binary diagrams with early work by Bernard et al. (1977), Schoell (1983), Whiticar et al. (1986) and recent refinement by Milkov and Etiope (2018). Advances in microbiology have first enabled the identification and quantification of the microbial and archaeal species responsible for the generation of secondary biogenic methane and genome directed metabolism analysis has enabled the identification of the various metabolic pathways involved in methanogenesis; for example, determining that CO_2 reduction is the dominant pathway in the Walloon Subgroup (WSG) (Evans et al., 2015). Although it is acknowledged that while these microbes are present in the groundwater it is not known if they are active or dormant (P.N. Evans, personal communication).

Most CBM is classed as secondary biogenic, as it is produced post-coalification at lower temperatures (< 56 °C) via two main pathways, acetoclastic fermentation or CO_2 reduction (Strapoc et al., 2011; Whiticar et al., 1986), with each pathway resulting in relatively distinct stable isotopic compositions (Golding et al., 2013). Consequently, microbial processes (sulfate reduction, methanogenesis) result in specific stable isotope signatures such as enriched δ^2H-H_2O values, as well as enriched δ^{13}C-DIC and $\delta\ ^{13}$C-CO_2 values. They also influence the groundwater major ion composition resulting in high Na, and HCO_3 with comparably low SO_4, Ca, Mg. These distinctive, common chemical and stable isotopic compositions are regardless of age or formation lithology (McIntosh and Martini, 2008; Van Voast, 2003).

While the study of the microbial processes and identification of microbial consortia by metagenomics has arguably reached maturity and the gross composition of the associated groundwater is understood, there are still knowledge gaps in considering the impact of the additional fluid-rock interactions that occur within host lithologies. This is especially the case with Australian CBM basins. Strontium isotopes have been used to trace solute sources, fluid migration and local water-rock

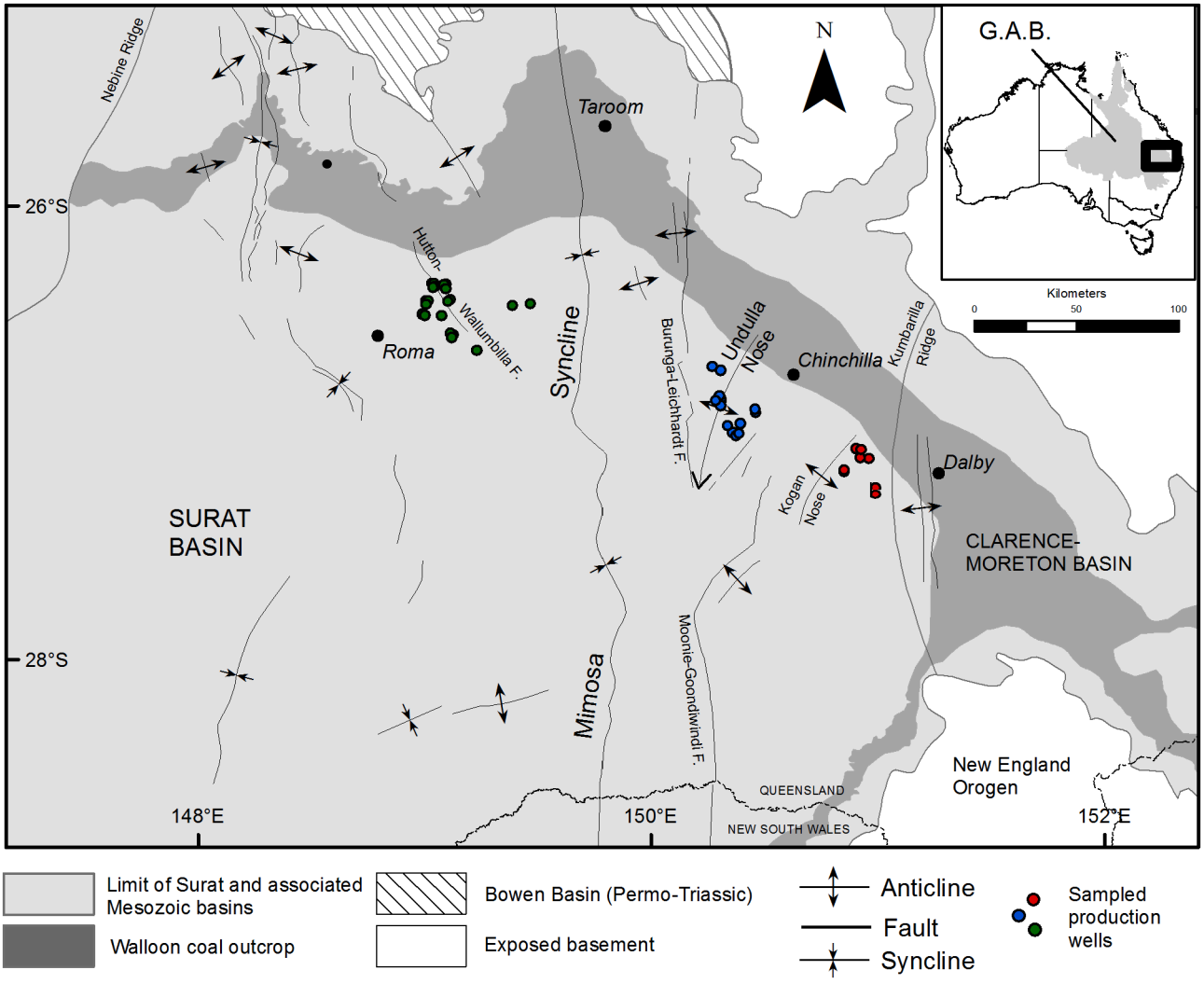

Fig. 1. Structural elements map of the study area, showing the three locations (Roma-green, Undulla Nose-blue, Kogan Nose-red) of Walloon CSG production wells sampled for gas and water. Inset: Location of the study area within Australia and the Great Artesian Basin. (For interpretation of the references to colour in this figure legend, the reader is referred to the web version of this article.)

interactions such as silicate weathering (Armstrong et al., 1998; Baublys et al., 2019; Capo et al., 2014; Stueber et al., 1987), but further investigations into identifying other low temperature processes are still needed. This work focuses on the Walloon Subgroup of the Surat Basin in Queensland, Australia (Fig. 1). CBM discovery was much later in Australia than the USA and commercial production in the Surat Basin did not commence until 2006. As such, there is much unknown with regards to the impact on the groundwater resources and most hydrogeochemical processes are still poorly understood. Studies by Australia's Commonwealth Science and Industry Research Organisation (CSIRO) and others have demonstrated that groundwater flow patterns in the Surat Basin, recharge and aquifer-interconnectivity are more complex than previously postulated (Hodgkinson and Grigorescu, 2013; OGIA, 2016, 2019; Ransley and Smerdon, 2012; Suckow et al., 2020; Vink et al., 2020). This work challenges the traditional view of groundwater being recharged in the east of the Surat Basin and mostly flowing to the west into the deeper Great Artesian Basin. In this context, the intake beds along the eastern margins of the Surat Basin have long been assumed to serve as a major site of recharge for the Great Artesian Basin. Hamilton et al. (2014a) have hypothesized that recharge along these eastern margins is responsible for the injection of methanogens to start secondary methane production some 50,000 years ago based on ^{14}C data reported in Baublys et al. (2015). Although interpretations of the ^{36}Cl data herein show that the time was significantly underestimated.

In this study, we examine the likely fluid-rock and microbial interactions that result in the current composition of the Walloon Subgroup co-produced groundwater from CBM production wells, using tracers (^{14}C, ^{36}Cl, $^{87}Sr/^{36}Sr$, $^{18}O/^{16}O$, $^{13}C/^{12}C$), hydrochemical and geochemical data. The tracer data is interpreted via a process-based approach, where we discuss different scenarios and the influence of low temperature fluid-rock interactions such as cation exchange, hyperfiltration and matrix diffusion responsible for the composition of the groundwater. We show that the Walloon Subgroup essentially functions as a stagnant aquitard and that the typical composition of the coal seam gas production water is slowly being imprinted by the effects of low temperature fluid-rock interactions. Gas and groundwater chemistry data from CBM production wells are not readily available and constraints around the difficulty of accessing and sampling CBM production wells have led to very few studies that improve the understanding of CBM groundwater geochemistry and associated formation characteristics. This study provides an in-depth analysis of rare gas and groundwater chemistry data in the context of coal formation hydrogeology.

2. Setting

The Mesozoic Surat Basin in Queensland, Australia, is one of the larger CBM producing basins in the world with reserves of 25,500 petajoules (DNRME, 2019). It is part of Australia's Great Artesian Basin and comprises a series of aquifers and aquitards from the surface to ~2000 m depth in the central part of the basin. Coal bed methane is produced from the Middle Jurassic Walloon Coal measures, a unit underlain by sandstone units that are the major source of potable water for much of semi-arid Queensland and that are heavily relied on (Fig. 2).

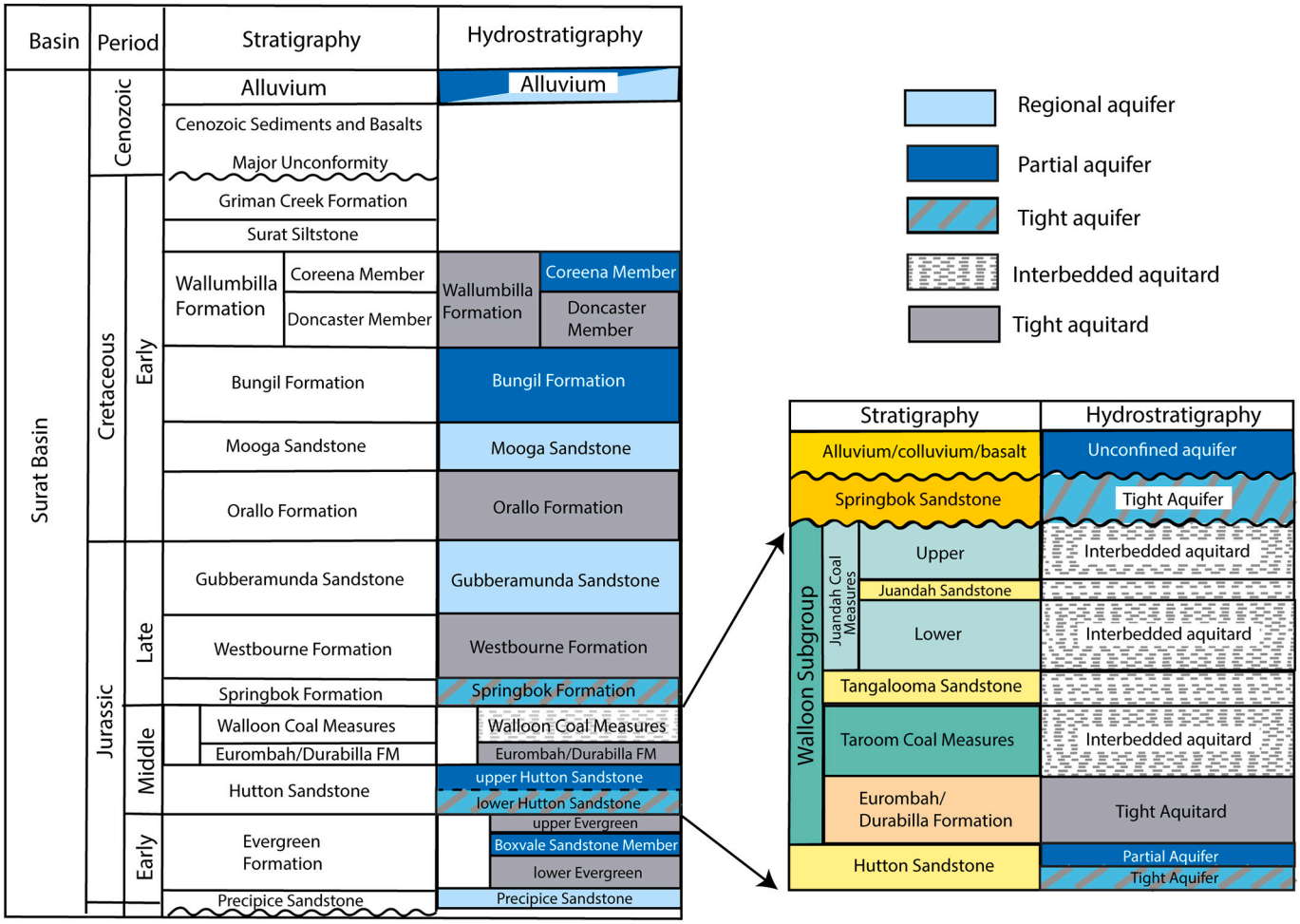

Fig. 2. Walloon Subgroup stratigraphic subunits, hydrologic units and over- and underlying aquifers in the study area. Adapted from OGIA (2019), Baublys et al. (2015).

2.1. General hydrogeology

The Surat Basin evolved in a continental sag sedimentary basin setting where fluvio-lacustrine strata dominate the lower part of the sedimentary sequence, while the upper part records a marine transgression followed by shallow marine and coastal plain deposition (Exon, 1976). The northern and eastern margins of the Surat Basin provide one of the main sources of recharge for the GAB (Habermehl, 2002) although the extent of recharge along these margins is currently under discussion (OGIA, 2019; Suckow et al., 2020; Suckow et al., 2018; Vink et al., 2020).

The focus of this study is the Walloon Subgroup strata in the north-eastern section of the Surat Basin that host the CBM. The strata dip gently (<5°) towards the Mimosa Syncline in the central eastern part of the basin and range in thickness from <300 m near Roma to >500 m east of the Mimosa Syncline (Hamilton et al., 2014b). The subgroup is relatively undeformed with only minor brittle faults and low-amplitude folds including two anticlines, the Undulla Nose and the Kogan Nose, which formed in response to reactivation of the Permian-Triassic Hutton-Wallumbilla, Burunga-Leichhardt and Moonie-Goondiwindi fault systems during and after the Late Cretaceous (Cook and Draper, 2013; Exon, 1976; Hodgkinson and Grigorescu, 2013; Korsch et al., 2009; Scott et al., 2004; Sliwa and Esterle, 2008) (Fig. 1).

The three CBM production regions in this study are located around deformations associated with these fault systems, the Hutton-Wallumbilla fault in the west (Roma), the Burunga-Leichardt fault in the east (Undulla Nose anticline) and the Moonie-Goondiwindi fault system in the southeast (Kogan Nose anticline) (Fig. 1).

The fluvio-lacustrine Walloon Subgroup is highly heterogeneous, comprising interbedded sandstones (litharenites, commonly with a smectite matrix and carbonate cement), shales, siltstones, mudstones, minor limestones, siderites, silicic ash-fall tuff horizons and coal seams (Supplementary Fig. 1). The coal seams comprise approximately 10% of the whole sequence. All the sedimentary beds of the subgroup, but particularly the coal seams, are laterally discontinuous and difficult to correlate across the basin (Hamilton et al., 2014b; Jell et al., 2013; Martin et al., 2013; Ryan et al., 2012; Scott et al., 2004). The subgroup is commonly divided into six sub-units: the relatively coal-free basal transition Durabilla Formation and three units, the Taroom Coal Measures, the Tangalooma Sandstone, and the Juandah Coal Measures, where the latter comprises upper and lower informal coal measure members separated by a sandstone interval (known as the Wambo Sandstone in the east and the Proud Sandstone in the west) (Hamilton et al., 2014b; OGIA, 2016) (Fig. 2).

Average coal permeability values range from <1 to >500 mD in the eastern study areas, and from ~50–200 mD in the Roma/west region, although locally higher values are possible (Ryan et al., 2012; Scott et al., 2004). Walloon Subgroup sandstones generally have poor reservoir characteristics (low porosity, generally <15%; permeability generally <2 mD) (Geological Survey of Queensland, G, 2013; Martin et al., 2013). Overall, there is significant spatial variability across the basin in coal geometry, type and lateral extent (Esterle et al., 2013; Hamilton et al., 2014b; Martin et al., 2013; Ryan et al., 2012).

2.2. General hydrogeochemistry

Walloon Subgroup CBM wells are mainly vertical wells targeting multiple coal seam intervals in both the Juandah and Taroom coal measures. These coal seam intervals are split by very thinly interbedded carbonaceous mudstones and tuff horizons, but more commonly also contain siltstone, claystone and sandstone. As such, CBM water samples come from mixed sources across several perforated coal seam intervals over approximately 300 m, across at least two Walloon sub-units (Baublys et al., 2015).

Co-produced waters from Surat Basin CBM wells are brackish with the typical CBM groundwater composition of low sulfate and magnesium and elevated HCO_3, Na and Cl (Baublys et al., 2015). However, each production region has distinct geochemical characteristics that have been attributed to the differences in adjacent subcrop lithologies (Baublys et al., 2015). The Roma region outcrop is relatively unobscured while the eastern regions are overlain by Quaternary sands. Consequently, the western Roma wells are the freshest with the lowest total dissolved solids (TDS) ranging from 1433 to 5906 mg L^{-1} (average 2738 mg L^{-1}) and relatively low alkalinity ($CaCO_3$), ranging from 372 mg L^{-1} to 1090 mg L^{-1}, average 788 mg L^{-1}. In contrast, the shallower, Undulla Nose groundwaters on the eastern side of the basin have moderate TDS values (average 3645 mg L^{-1}) but double the alkalinity (average 1566 mg L^{-1}). The south-eastern Kogan Nose wells are the shallowest of the three production areas (Table 4.1) and have the highest TDS and mid alkalinity values (average TDS: 5286 mg L^{-1}; average alkalinity: 1247 mg L^{-1}). Here, the groundwaters are Na—Cl dominant type, whereas the Roma region and Undulla Nose groundwaters are predominantly of Na-HCO_3 type.

3. Sampling and analytical methods

This study forms the final stage in analysis and characterisation of the CBM production groundwaters in the WSG of the Surat Basin (Baublys et al., 2015, 2019). Initial gas isotopic, hydrochemical and co-produced groundwater tracer data (δ^{13}C-CH_4, δ^{2}H-CH_4, δ^{13}C-CO_2, δ^{18}O-H_2O, δ^{2}H-H_2O, alkalinity, Na, Ca, Mg, Cl, SO_4, F, N, P, Sr, $^{87}Sr/^{86}Sr$, δ^{13}CDIC) for 51 CBM production wells (Fig. 1) were presented in Baublys et al. (2015 and 2019) along with detailed sampling methods. Of these wells a subset of 18 were selected for ^{36}Cl measurement and 30 for ^{14}C (Table 1). In addition to the groundwater samples from CBM wells, select water compositional data (Cl, δ^{18}O-H_2O) from 7 shallow monitoring bores located on the edge of the northern subcrop were recently supplied by Queensland Gas Corporation. Locations are shown on the map in Fig. 6 and subsequent plots as black circles.

Over the lifetime of this study, ^{14}C and ^{36}Cl analyses were carried out across two facilities, one contracted by CSIRO and the Australian Nuclear Science and Technology Organisation (ANSTO). For the ^{14}C analysis undertaken with CSIRO, 5 L of water were collected in HDPE jerry cans and the unfiltered samples were sent to the CSIRO isotope laboratory in Adelaide for preparation using the method of Leaney et al. (1994). Precipitates were then analysed at the Australian National University Radiocarbon Dating Centre using single stage accelerator mass spectrometry (SSAMS) as per Fallon et al. (2010). Samples at ANSTO were processed as follows. Following acid extraction and graphitisation of inorganic carbon, ^{14}C concentrations were analysed using accelerator mass spectrometry (2MV VEGA tandem accelerator). The concentrations for ^{14}C are expressed as percent modern carbon (pMC) and the 1σ error of $^{14}C/^{12}C$ ratios is ±0.16% with all calculations following the protocols of Stuiver and Polach (1977). In this study, variations in CSG well construction across sites, environmental and occupational health and safety laws sometimes constrained sampling procedures and possibilities. As such minor atmospheric contamination was considered a possibility and precluded in-depth interpretation of very low pMC levels. Consequently, ^{14}C pMC values are uncorrected for any additions of 'dead' carbon (^{14}C free carbon).

^{36}Cl/Cl ratios were determined by both CSIRO and ANSTO via AMS with the CSIRO samples being analysed at the Australian National University using the 14UD accelerator with techniques detailed by Fifield (1999). ANSTO samples were also measured by AMS on 6MV SIRIUS Tandem Accelerator (Wilcken et al., 2017). Analytical error for all ^{36}Cl is between 4 and 10%. For ease of expression, the ^{36}Cl/Cl ratios (the ratio of ^{36}Cl to total Cl × 10^{-15}) is hereafter referred to as R^{36}Cl and multiplied by 10^{+15}.

To allow for better assessment of the ^{36}Cl ratios, 3 rainwater samples from the Roma and Chinchilla areas were also analysed for their ^{36}Cl ratios to act as a proxy for determining the surface or atmospheric input of ^{36}Cl. As the study area is semi-arid it is difficult to collect enough

Table 1
Cosmogenic tracer and selected hydrochemical data for the Walloon Subgroup CBM production wells across Roma, Undulla Nose and Kogan Nose production regions.

Well name	Distance	Mid-point	$\delta^{13}C_{DIC}$	^{14}C	error	$R^{36}Cl$	error	$A^{36}Cl$	Cl	TDS	$\delta^{18}O\text{-}H_2O$
	km	depth m	‰VPDB	pMC		$x10^{-15}$	$x10^{-15}$	*10–7	mg L^{-1}	mg L^{-1}	‰VSMOW
Undulla Nose											
BV-3	14	323	15.7	0.21	0.11	12.2	1.3	34.10	1650	4741	−8.6
BV-9	15	357	19.7	0.12	0.05	–	–	–	1040	3826	−9.0
AG-13	30	438	13.4	0.20	0.11	–	–	–	443	3597	−8.0
AG-31	29	435	11.7	0.15	0.05	14.1	1.4	18.90	790	3820	−8.2
BS-19	27	464	13.3	0.13	0.05	–	–	–	540	2694	−7.6
BS-36	26	463	13.9	0.12	0.05	14.5	1.3	18.90	770	3947	−8.4
BS-41	25	459	14.7	0.27	0.03	–	–	–	547	2410	−7.1
BS-48	29	511	14.8	0.85	0.04	–	–	–	537	3362	−7.7
BS-90	28	506	17.9	0.24	0.05	–	–	–	838	3390	−8.0
CD-2	34	638	14.7	–	–	–	–	–	303	3832	−7.4
CD-14	44	620	7.5	0.18	0.03	–	–	–	326	3332	−7.6
CD-6	44	643	17.4	0.12	0.02	14.3	1.3	8.61	355	4723	−7.6
CD-10	35	632	17.1	–	–	–	–	–	352	3912	−7.5
CD-8	42	632	15.1	0.33	0.05	14.7	1.4	8.23	330	3697	−7.4
LN-24	37	495	12.4	0.32	0.03	–	–	–	516	3647	−7.5
LN-47	34	578	12.7	0.19	0.03	12.2	1.2	6.52	315	3391	−7.5
Kogan Nose											
RJ-8	23	482	20.4	0.31	0.05	–	–	–	2580	6218	−8.8
RJ-9	22	490	14.2	0.33	0.05	12.4	1.3	44.14	2100	5706	−8.7
BW-166	14	379	20.3	–	–	–	–	–	1360	4551	−7.3
BW-3	15	381	19.6	–	–	14.6	1.5	40.18	1620	4804	−7.2
BW-185	16	400	22.1	0.33	0.09	–	–	–	1870	5342	−7.5
DV-4	16	449	21.1	0.27	0.10	10.0	0.8	25.08	1480	5112	−7.5
DV-2	15	430	21.4	0.28	0.10	–	–	–	1750	5625	−7.5
DAA-43	10	312	–	–	–	–	–	–	1050	4431	−7.1
DAA-45	13	290	–	–	–	–	–	–	1730	4699	−5.9
KO-37	12	203	–	–	–	–	–	–	2460	5164	−6.4
KO-12	10	150	–	–	–	–	–	–	3580	6491	−5.9
Roma											
East HW											
CK-2	13	272	–	–	–	–	–	–	426	2184	−6.9
CK-4	14	312	–	–	–	–	–	–	632	2300	−6.8
CK-10	16	321	25.9	0.15	0.05	16.1	1.4	14.75	539	2601	−7.2
MH-4	21	391	–	–	–	–	–	–	550	2120	−7.1
MH-5	22	390	–	–	–	–	–	–	372	1413	−6.6
MH-6	20	382	17.8	1.12	0.03	10.1	1.0	13.25	772	3111	−7.1
West HW											
HM-12	13	533	18.2	–	–	–	–	–	1100	2926	−7.0
HM-3	13	536	16.1	0.85	0.04	23.8	1.7	32.66	810	2620	−6.9
HM-4	15	514	–	–	–	–	–	–	728	2424	−6.9
HM-7	15	522	–	–	–	–	–	–	555	2514	−6.9
PR-20	29	535	–	–	–	–	–	–	550	1937	−6.9
PR-21	29	526	–	–	–	–	–	–	519	1948	−7.0
PH-27	22	455	–	–	–	–	–	–	582	2139	−6.9
PH-28	22	486	17.8	1.32	0.03	11.2	0.7	16.10	846	3285	−6.9
PH-29	24	504	–	–					763	2841	−7.0
RA-8	29	629	18.8	0.92	0.03	9.0	0.8	6.35	982	3296	−7.1
RM-8	26	520	18.8	1.95	–	–	–	–	746	2840	−6.9
PJ-13	38	725	–	–	–	–	–	–	355	1723	−7.0
PJ-18	38	713	–	–	–	–	–	–	588	2102	−6.9
PJ-20	38	862	–	–	–	–	–	–	379	1728	−6.8
PJ-28	40	711	15.7	1.02	0.06	13.9	1.4	29.69	1240	3426	−7.2
away HW											
BB-3	32	675	16.8	0.33	0.05	12.8	1.3	37.59	1730	4349	−7.9
WP-3	48	826	14.2	0.26	0.05	11.2	1.3	29.34	1540	3968	−7.6
TD-4	29	614	16.7	0.52	0.03	9.9	1.0	45.42	2700	5906	−7.9
Tank rainwater											
2 Chinchilla		–	–	–	–	116.8	5.0	0.20	1	–	−4.3
3 Roma		–	–	–	–	109.3	5.1	0.44	2	–	−2.6
4 Roma		–	–	–	–	139.7	6.0	0.45	2	–	−1.9
Miles Rain		–	–	–	–	–	–	–	–	–	−4.6

rainwater for ^{36}Cl analysis, thus samples were drawn from long-term rainwater storage tanks from the towns of Roma and Chinchilla.

4. Results

4.1. Radiometric carbon activity (^{14}C)

The ^{14}C activities (pMC) are uniformly low across all 3 production regions (0.12–1.93) with a median value of 0.3 (Table 1). While modern instruments now allow precise measurements below 1 pMC, it is

generally accepted that when interpreting ^{14}C values in groundwater, levels below 1 pMC are not significant and cannot be easily interpreted (Cartwright et al., 2020). However, it can be assumed that ^{14}C values in groundwater below 1 pMC can represent residence times well above 30,000 years and therefore cannot be easily interpreted (Cartwright et al., 2020). Therefore, the pMC values here have not been corrected for any contributions from 'dead', non-radiogenic carbon arising from, for example, dissolution of carbonate minerals or HCO_3 from SO_4 reduction.

However, some broad observations are still possible. The Undulla Nose region has the lowest median value at 0.2 pMC with a range of 0.12 (±0.02) – 0.84 (±0.04)), which is similar to the nearby Kogan Nose with a median value of 0.3 and a range of 0.27 (±0.1) – 0.33 (±0.05). The Roma samples have the largest range 0.15 (±0.05) – 1.93 (±0.03) and a median value of 0.7, which is significantly higher than the production areas on the eastern side of the basin.

4.2. ^{36}Cl activity

The $R^{36}Cl$ values of the production waters range from 9.02 to 23.77 across all 3 production locations with groundwater in the Roma region exhibiting both the highest and lowest values (Table 1). The 3 samples from the Kogan Nose are 9.99, 12.39 and 14.62. Undulla Nose samples cover a narrower range from 12.2 to 14.7 ($n = 6$), which are almost indistinguishable when analytical errors are considered (Fig.3b). All wells located 17 km or further from the subcrop have essentially the same $R^{36}Cl$ values (Figs. 3a, 5). Only two wells have elevated $R^{36}Cl$ values (23.8, 16.1) and both are in the Roma region and are located close to the subcrop (13 km and 16 km). These wells are screened over the same intervals of the WSG as the other Roma wells. There is no correlation of $R^{36}Cl$ values with TDS, Cl concentration or pMC. The maximum flow distance from nearest subcrop is 48 km.

4.2.1. $A^{36}Cl$

Whereas $R^{36}Cl$ values are not affected by concentration through evaporation, $A^{36}Cl$ values (which represent the concentration of ^{36}Cl atoms per litre, usually multiplied by 10^7 for ease of expression) are affected by evaporation and/or transpiration. WSG production water values range from 6.4 to 45.4 (Table 1) with the Roma area again having the lowest and highest values. Undulla Nose values range from 6.5–34.1, while the Kogan Nose values range from 25.1–44.1. Rainwater from the region was measured with an $A^{36}Cl$ of 0.36 and is taken as an approximation of recharging groundwater with acknowledgment that it has not been subject to the same processes as recharging water e.g., concentration through evapotranspiration processes at the surface and in the shallow soil profile. All co-produced groundwater samples from all 3 areas exhibit the same positive correlation of increasing $A^{36}Cl$ with increasing Cl concentration (Fig. 4), indicating that this increase is likely from surface evaporation and/or transpiration processes rather than mixing with other groundwater.

5. Discussion

Cosmogenic tracers ^{14}C and ^{36}Cl are often used together, as the presence of measurable ^{14}C with low $R^{36}Cl$ can indicate mixing of groundwaters with different residence times, e.g., adjacent aquifers (Cartwright et al., 2020; Iverach et al., 2017). While it is acknowledged that groundwater flow distances in this study are short (13–48 km from subcrop) and that methanogens and sulfate reducers dilute the ^{14}C pool with non-radiogenic or 'dead' carbon (Clark and Fritz, 1999; Van Voast, 2003), it was presumed that there would still be significant pMC present rather than the very low levels discovered. This was inferred from ^{14}C values measured for the overlying Springbok Sandstone in the Kogan Nose area (1.8 and 2.9 pMC, Caffery unpubl. Data, see acknowledgements) and the nearby Condamine Alluvium (average ^{14}C of 48.0 pMC (Scheiber et al., 2020)). Hence, it was unexpected that the $R^{36}Cl$ values were also very low. Two main concepts are explored in this discussion. Firstly, the reason for the low, ^{14}C and $R^{36}Cl$ values, and secondly the implications of these low cosmogenic isotope concentrations for the interpretation of the hydrochemical data, with a focus on the $\delta^{18}O$ and Cl (Baublys et al., 2015) with subsequent and additional of low

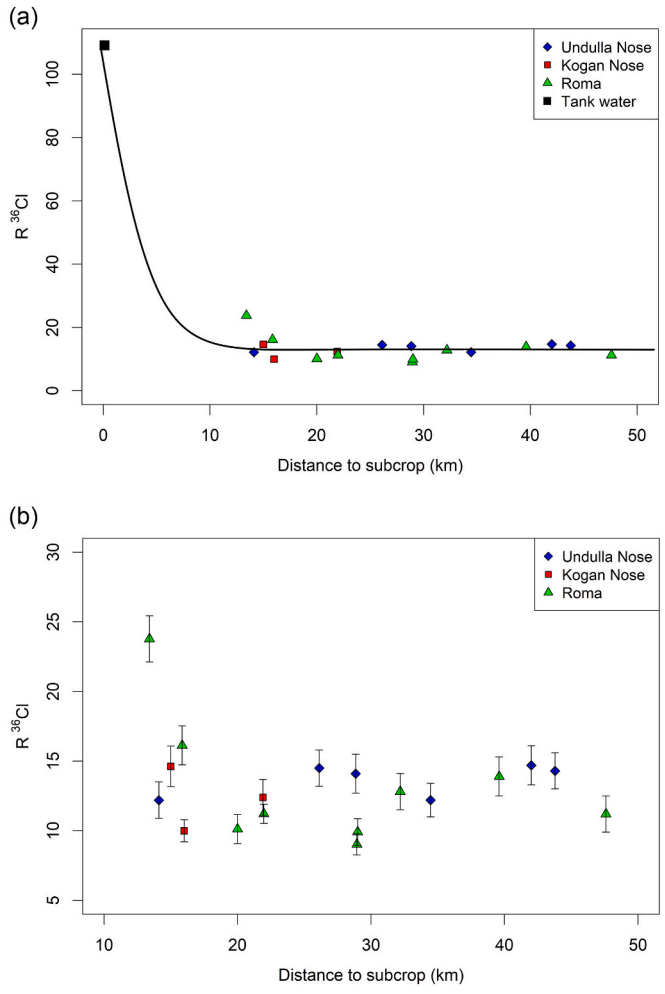

Fig. 3. (a) Decline of WSG $R^{36}Cl$ production waters over distance with the black square denoting modern meteoric average for the region. (b) Enlarged section showing error bars for production waters.

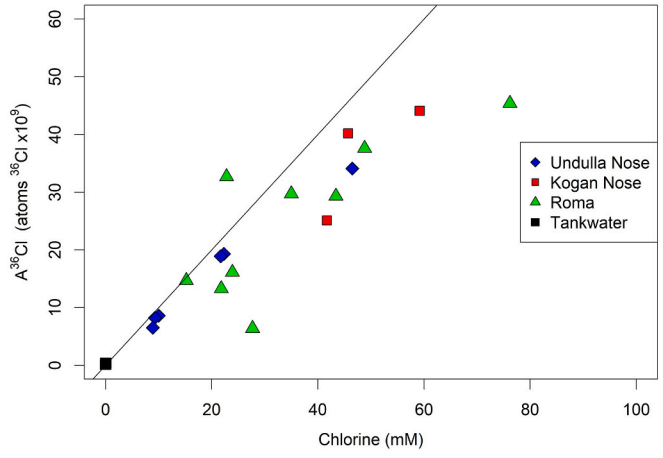

Fig. 4. All three production areas show same positive correlation between $A^{36}Cl$ atoms and Cl concentration indicative of evaporative and/or transpiration processes.

temperature fluid-rock interactions.

5.1. ^{14}C

Low pMC values in low-rank CBM reservoirs such as in this study can be the result of a combination of processes including natural decay, dilution of pMC values by the addition of '^{14}C-free' (non-radiogenic) carbon through processes such as calcite dissolution, sulfate reduction, methanogenesis, addition of geogenic CO_2 or ^{14}C loss. A potential loss of ^{14}C can occur through matrix diffusion into isolated pore spaces (Clark and Fritz, 1999; Davidson and Airey, 1982; Suckow et al., 2020). While these processes complicate the interpretation and the calculation of mean residence times of the groundwater, they do provide important information on the geochemical processes related to reservoir behaviour and possible fluid-rock interactions. In general, dilution or loss of ^{14}C results in an overestimation of mean residence times of groundwaters (Cartwright et al., 2020).

The groundwaters in this study have been heavily influenced by biogenic processes of sulfate reduction and methanogenesis (CO_2 reduction) indicated by positive δ^{13}C-DIC values (average 17‰), low to no detectable SO_4 and high alkalinity concentrations (average. 1131 mg L^{-1}) (Baublys et al., 2015). While both processes, sulfate reduction and methanogenesis, are likely to be significant contributors of ^{14}C free carbon to the dissolved inorganic carbon (DIC) pool, they are not necessarily the only processes contributing to the low ^{14}C values. Two other processes can be responsible for ^{14}C-dilution. Firstly, carbonate dissolution can also add ^{14}C-free carbon but the mostly positive saturation indexes (calcite ~0.3, dolomite ~0.5) are more indicative of carbonate precipitation rather than dissolution (Baublys et al., 2019). As well, Ca/Cl ratios of the CBM groundwater are much lower (0.009 avg.) than either local rainfall (1.3) or marine (0.037) values indicating that carbonate dissolution is unlikely. Secondly, a source of ^{14}C free carbon can originate from vertical leakage through aquitards and aquifers of older or stagnant water. CBM water samples are drawn from wells screened across the coal bearing sections of the WSG and are themselves an average composition of the WSG groundwater. However, the WSG with its many interlayers of mudstone, siltstones and high clay content throughout, has a low vertical hydraulic conductivity (4.8×10^{-8} m/day) (OGIA, 2016) that makes mixing with groundwater from adjacent geological units, the Springbok Formation above and the Durabilla Formation below, and hence the possibility to mix with older waters as a source of dead carbon, unlikely.

Correction techniques that involve mass balance models based on DIC concentrations or δ^{13}C isotope values can be applied to correct for the addition of non-radiogenic carbon but these techniques cannot separate carbonate dissolution from the biogenic addition of carbon, as both increase DIC concentration and δ^{13}C values. However, carbonate dissolution must occur in significant quantities to influence DIC concentrations and δ^{13}C values which are overprinted by methanogenic processes. Marine carbonates have a δ^{13}C of around 0‰ and dissolution of carbonates would raise the δ^{13}C values but the final groundwater δ^{13}C cannot exceed 0‰, even if significant amounts of carbonates were dissolved. The presence of low Ca/Cl ratios of the sampled groundwater (<0.011), similar to or smaller than ocean water (~0.02), and the absence of calcite bearing rock formations in the recharge areas also suggest minor influences of carbonate dissolutions. The high positive δ^{13}C therefore suggests that biogenic SO_4 reduction and methanogenesis are the main processes contributing non-radiogenic carbon in addition to the natural decay.

Additionally, the constraints around sampling CBM wells, as described in the methods section, may have caused a small amount of atmospheric CO_2 contamination, which may have resulted in slightly higher pMC values.

5.2. ^{36}Cl

^{36}Cl is not influenced by the same biogenic processes as those affecting radiocarbon but is subject to fluid-rock interaction processes. First though, it is argued that the R^{36}Cl values for the WSG have reached secular equilibrium. Secular equilibrium (R_{SE}) is defined as the R^{36}Cl value at which in-situ production of ^{36}Cl in the subsurface (hypogenic) is matched by its decay and is often theoretically set to 5 half-lives (Clark and Fritz, 1999). This value can slightly changed depending on local subsurface conditions and mineralogy, as some conditions can produce low levels of ^{36}Cl via the absorption of thermal neutrons produced by uranium fission and uranium-thorium series decay (Lehmann et al., 1993; Phillips, 2013). R_{SE} levels of 5 to 10 have been reported for the Great Artesian Basin (Bentley et al., 1986; Lehmann et al., 2003; Mahara et al., 2009; Suckow et al., 2016). However, these values have been determined in sandstone aquifers of the Great Artesian Basin such as the Hooray Sandstone and Algebuckina Sandstone in the central and western regions (Mahara et al., 2009) which do not contain the high levels of clay and organics as the WSG. As clays and organic materials such as coal are well known for having higher radioactivity levels than sandstone (Mathew, 1979), it could be argued that the R_{SE} of the WSG would be higher than that of the sandstone units of the Great Artesian Basin.

As R^{36}Cl values in this study are relatively constant from ~16 km from the subcrop region onwards (Figs. 3a, 5), it is likely that the values for the WSG have reached secular equilibrium (average. 12.3). This value is higher than that for the overlying Springbok Sandstone (R^{36}Cl average 7.0) due to the likely presence of higher levels of uranium (thermal neutrons produced during decay produce low levels of ^{36}Cl) in the WSG compared to Springbok Sandstone. The low R^{36}Cl values so close to the subcrop are unusual compared to other formations but there are several possible scenarios as to why the R^{36}Cl have reached such low levels over short groundwater flow distances: 1) Groundwater flow-paths and/or flow directions assumptions are incorrect; 2) Mixing with older waters; 3) Groundwater is old and tracer loss is the result of natural decay; and/or 4) Loss of cosmogenic tracers through matrix diffusion/dual-porosity or hyperfiltration.

5.2.1. *Incorrect groundwater flow paths*

Early work on Great Artesian Basin flow systems assumed that the margins of the Surat Basin served as major recharge areas (Bentley et al., 1986; Habermehl, 2006; Smerdon et al., 2012) and as such groundwater flow distances from assumed recharge areas for this study were measured from the production well to the nearest subcrop, which are groundwater flows from the Great Dividing Range in the north and east towards the south and the west, respectively. These historic conceptions of groundwater flow in the basin were mainly based on the single sandstone aquifers. Groundwater flow and recharge in the WSG was assumed to follow similar patterns (Fig. 6).

However, the release of hydraulic pressure data for the WSG (OGIA, 2016, 2019), the lack of any known discharge areas, and the discovery of a hydraulic pressure divide along the northern margin of the WSG, demonstrates that groundwater flow patterns are not as simple as previously assumed and flow diversions towards the east are postulated for some of the sandstone aquifers as well (Hodgkinson et al., 2010; Ransley and Smerdon, 2012; Suckow et al., 2018; Vink et al., 2020) (Fig. 6).

Although the hydraulic contour maps are generated from pre-CBM water extraction well data, they still likely reflect anthropogenic influence due to a long history of water extraction for agriculture that predates CBM extraction by many decades (Smerdon et al., 2012). Thus, interpretation of past flow paths using pressure maps is complicated. While there is the possibility of much longer groundwater flow-paths in the western Roma region, the groundwater flow systematics for the eastern side of the WSG appear more complex. The major ion data for the Roma region indicate that the Hutton-Wallumbilla Fault acts as a barrier to groundwater flow, as demonstrated by the differences in concentrations of the major element data on both sides (Baublys et al.,

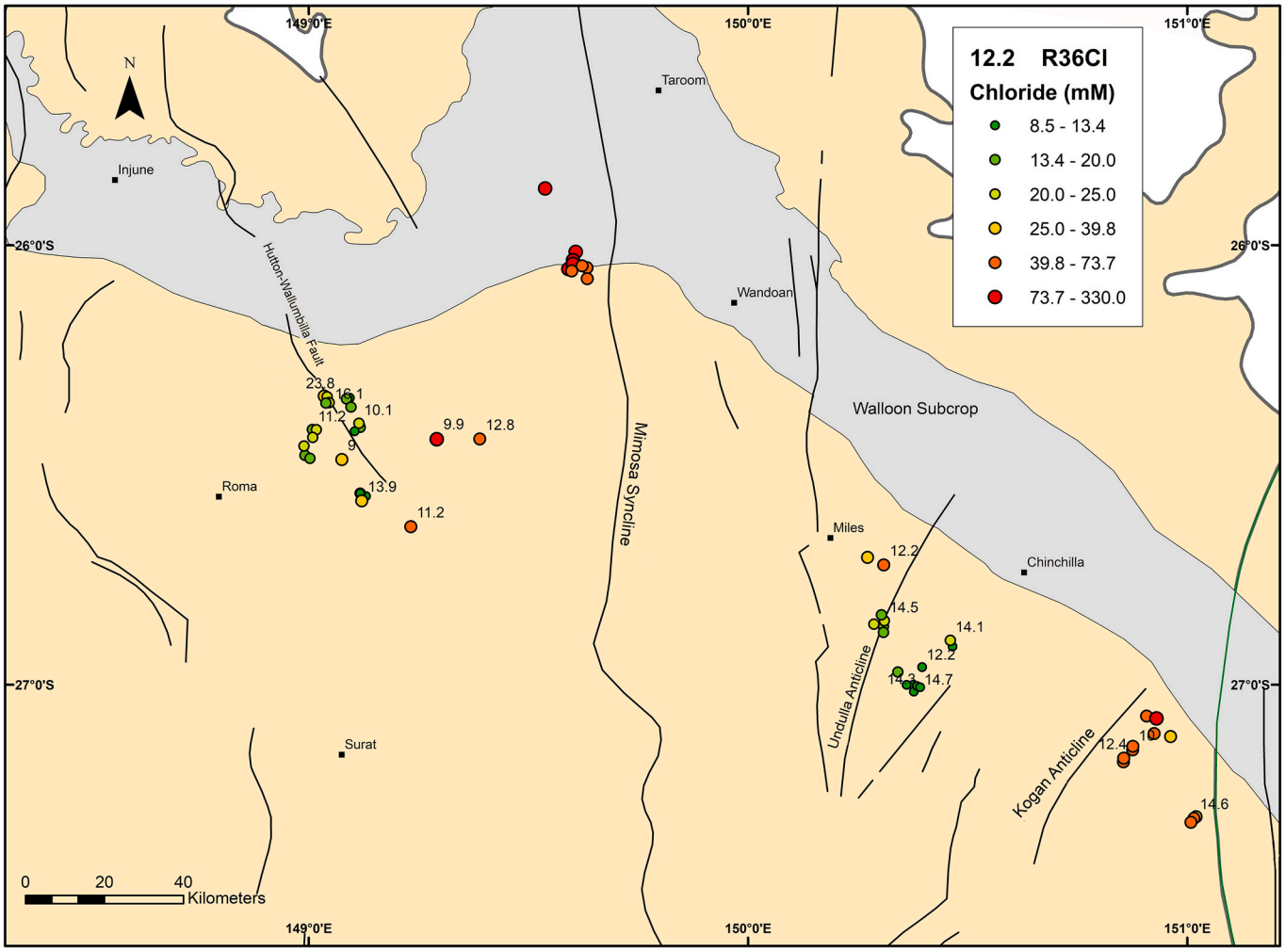

Fig. 5. $R^{36}Cl$ and Cl concentration trends across the Walloon Subgroup. The coloured circles indicate Cl concentration while the numbers indicate $R^{36}Cl$ values.

2019). If, as the hydraulic pressure data indicate, substantial recharge for the northern WSG was from the northwest rather than from the nearest subcrop, then it could be expected that the $R^{36}Cl$ data on either side of the fault would be more distinct (Figs. 5 and 7). Given the $R^{36}Cl$ data are essentially the same across all 3 production regions across the WSG, incorrect flow-path distances are unlikely; although the low horizontal groundwater flow velocities combined with the $R^{36}Cl$ at R_{SE} levels make definitive assertions impossible.

5.2.2. *Mixing with older waters*

This is unlikely as correlations of $R^{36}Cl$ and the number of atoms/L of ^{36}Cl ($A^{36}Cl$ - absolute concentration of ^{36}Cl per litre) vs Cl concentration (Figs. 4 and 7) indicate the major source of Cl is from meteoric water. Concentration increases in Cl derive in the absence of halite dissolution from transpiration rather than evaporation, as shown by the absence of any evaporation enrichment in the $\delta^{18}O$ and $\delta^{2}H$ data (Baublys et al., 2015). Additionally, there is no indication of any significant influx of groundwater on a regional scale, from either the overlying Springbok or the underlying Hutton Sandstone aquifers (OGIA, 2019). Chloride sources and sinks will be explored further in this paper.

5.2.3. *Groundwater has long residence times*

If the $R^{36}Cl$ do accurately reflect groundwater with very long residence times then the transmissivity of the WSG must be that of an aquitard. This is reflected by the recent classification by OGIA of the WSG as an 'interbedded aquitard' due to the many alternating beds of mudstone, siltstone, coal, sandstone, and tuff.

The hydraulic conductivity of the Walloon Subgroup is low overall; however, there is a great variation within the subgroup. For example, OGIA (2016, 2019) report horizontal hydraulic conductivity values (Kh) for the entire WSG at averages of 0.001–0.005 m/day but can be much greater for the individual coal plies with up to 1 m/day (OGIA, 2019). For comparison, the underlying Hutton Sandstone aquifer has a ranges two orders of magnitude higher with values of 0.1–0.5 m/day (CSIRO, 2014). WSG sandstone is ~0.005 to 1.4 m/day and the interburden is determined at 0.003 m/day (Moore et al., 2015; USQ, 2011). Consequently, using the ranges above, groundwater velocities are estimated at <0.1 m/y, which supports the idea of long mean residence times. By comparison, the estimated groundwater velocities of the underlying Hutton Sandstone are much larger at 0.7 m/y (Suckow et al., 2020).

Correlation of the coal plies across the WSG is difficult with maximum continuous distances of approximately 3000 m and flow in some instances blocked by the surrounding lower hydraulic conductivity units (Hamilton et al., 2014a). This would make any higher hydraulic conductivity present in the coal immaterial. Additionally, the WSG is a confined unit and is sealed below by the Durabilla Formation (OGIA, 2019). While general permeability is low, some areas of the WSG can supply enough water to be pumped for livestock, which illustrates that the transmissivity of the WSG is regionally variable. The presence of clay seals and coal seams interspersed with less permeable interburden shows that the WSG is extremely heterogeneous. With no known discharge areas, it can be argued that groundwater flow is negligible and

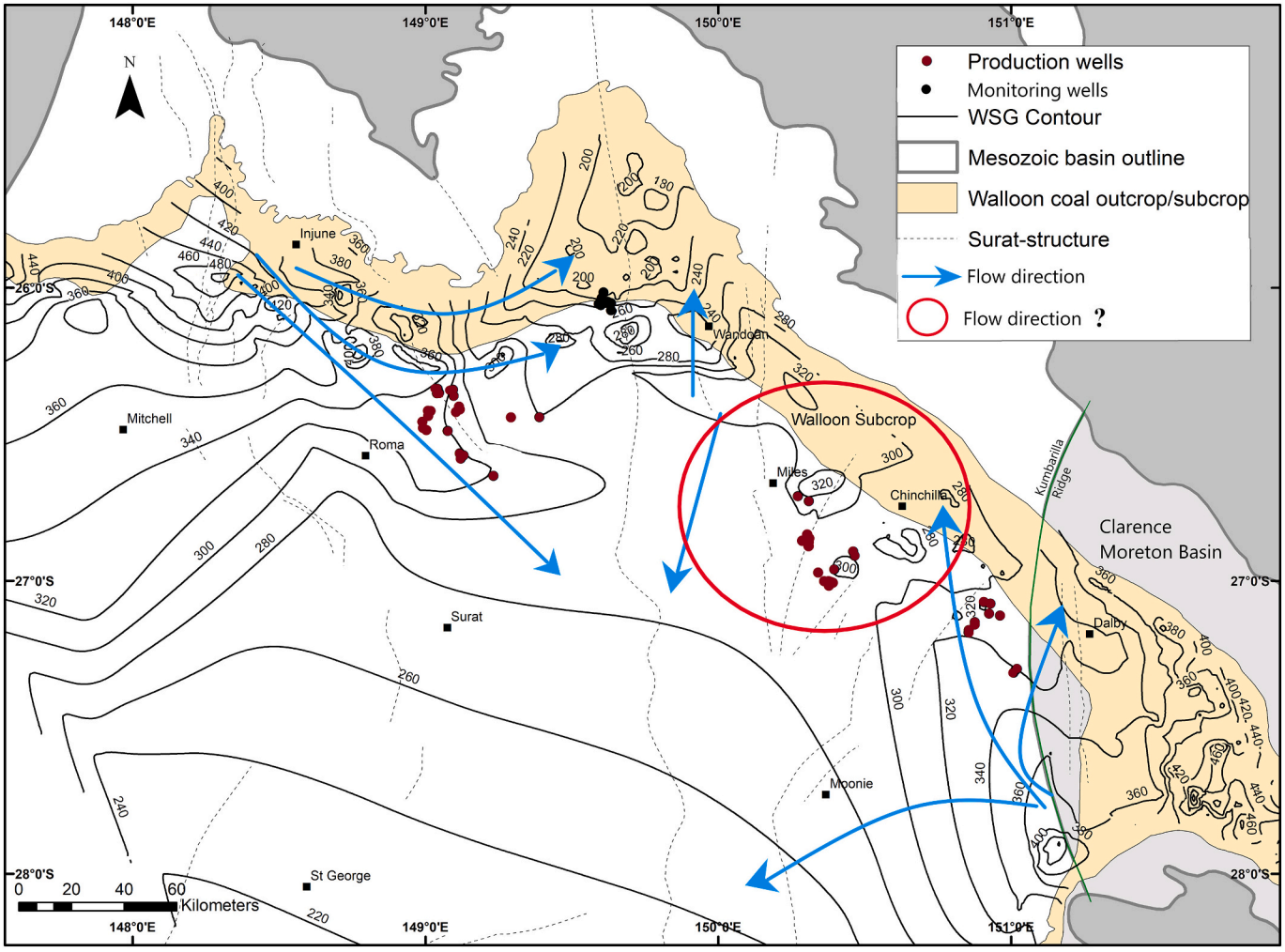

Fig. 6. Hydraulic pressure map of the Walloon Subgroup pre-CBM extraction but not pre-anthropogenic. Blue arrows indicate direction of flow with the red circle indicating Undulla Nose region where groundwater flow is under discussion. Contour overlay supplied by OGIA with contours in meters. (For interpretation of the references to colour in this figure legend, the reader is referred to the web version of this article.)

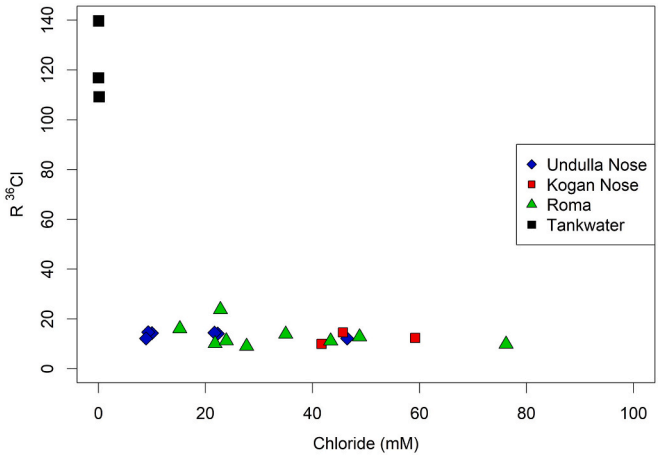

Fig. 7. $R^{36}Cl$ vs Chloride concentrations for the three production regions and local rainwater. Low $R^{36}Cl$ for all three regions with varying Cl concentrations indicating secular equilibrium.

that the uniformly low $R^{36}Cl$ values are a result of natural decay over time, which again supports the argument that the WSG is an aquitard or stagnant aquifer.

5.2.4. Loss of cosmogenic tracers

Apart from loss of ^{36}Cl through natural decay over time, ^{36}Cl can be lost through a process known as matrix diffusion in dual-porosity flow systems (Suckow et al., 2020; Sudicky and Frind, 1981, 1982; Winterle, 1998). For interbedded aquitards such as the WSG, dissolved solutes could be lost from units of higher permeability and flow within the WSG, for example flow along fractures or through the larger pores in sandstone, into the more stagnant pools and pores contained within units of lower permeability and porosity (mudstone, siltstone, tuff). Depending on the solute concentration gradients between areas of higher permeability (sandstones, coals) and those of lower permeability (claystones and mudstones), exchange occurs along the gradient by diffusion, forcing solutes into areas of lower concentrations. An example is the diffusion of dead Cl from the stagnant, low permeability pools back into the units of higher permeability, with the consequence of diluting the ^{36}Cl pool (Cartwright et al., 2020). However, this is considered unlikely as the groundwater flow in the WSG is predominately affected by its heterogeneity with poor lateral continuity of lithologies such as the coal, that can transmit water (Baublys et al., 2019; Hamilton et al., 2014a). Recent studies have identified this process in the underlying Hutton Sandstone aquifer (Suckow et al., 2020), which has much greater horizontal conductivity and is relatively more laterally continuous.

Effects from matrix diffusion can be assumed if vastly different flow velocities are obtained for each tracer, as calculated from plots of ^{14}C and ^{36}Cl against distance from subcrop. To determine velocity for each

tracer, the tracers are plotted exponentially against flow distance as measured from known recharge area (Suckow et al., 2020). A more comprehensive explanation is given in Suckow et al. (2020). The accurate calculation of flow velocities was not possible for this study due to the low levels of both cosmogenic tracers and short flow distances. However, the loss of cosmogenic tracers does mimic that found in the strontium isotope study of Baublys et al. (2019), which showed that levels of radiogenic strontium steadily decrease from the shallow subsurface to the production wells.

Diffusive processes are likely to be occurring at local levels within the WSG, such as between the units with higher permeability (coal and clean sandstones) and the units of lower permeability (mudstones and siltstones). The possible impact of this on the $R^{36}Cl$ of the groundwater is unknown as the direction of the Cl gradient is unknown.

In addition to matrix diffusion, other processes such as ultrafiltration need to be considered. Ultrafiltration, also known as hyperfiltration, is a process that has been hypothesized to affect Cl concentrations in groundwater and thus likely ^{36}Cl values. Ultrafiltration is essentially reverse osmosis where a semi-permeable membrane will allow the passage of some molecules while excluding others. In geological terms, it is any lithology which acts as a semi-permeable barrier to some solutes while excluding others (Hart et al., 2008). This would then result in the concentration of some solutes upgradient of the barrier and fractionation of isotopes across either side of the barrier lithology (Hart et al., 2008; Phillips and Bentley, 1987). Laboratory studies have shown that clays and shales can act as semi-permeable membranes by Hart et al. (2008) and references within. The process of ultrafiltration as applied to natural geological systems is still controversial as it is difficult to prove the effects in isolation when constraining large basin scale aquifers and aquitards (Hart et al., 2008). Within the larger geological scales, it is difficult to identify small scale processes like ultrafiltration especially when lithologies are extremely heterogeneous and the fact that natural systems are rarely ever static with a final steady state never reached (Neuzil and Person, 2017).

A further constraint is that ultrafiltration was thought to require a large hydraulic head difference as the main driver for the process across the clay or shale membrane (Neuzil and Person, 2017). However, Hart et al. (2008) have shown in laboratory studies that this can occur in dilute solutions at low hydraulic head pressures, which are present in the WSG. As well as retaining certain solutes, clay membranes can potentially fractionate isotopes such as ^{18}O, ^{3}H and ^{2}H of water, which can be retarded (Hart et al., 2008). In theory, retention of ^{18}O would result in higher $\delta^{18}O$ values upgradient and lower ones downgradient which would then show $\delta^{18}O$ values becoming more negative with distance. Kaolinite with its low cation exchange capacity has been shown to act as a membrane filter and it can be assumed that clays with higher cation exchange capacities are likely to be even more effective membrane filters (Neuzil and Person, 2017). Kaolinite and montmorillonite are ubiquitous across the WSG and are present in all lithologies (mudstone, siltstone, sandstone) (Baublys et al., 2019).

Chloride concentrations in the WSG drop within the first few kilometers of the subcrop (Fig. 8a) then start to again increase in both the Kogan Nose and Roma region. The increase is rapid for the Kogan Nose and much more gradual for the Roma region, while the Cl concentrations for the Undulla Nose remain low over similar flow distances. Strontium concentrations also follow the same trend (Fig. 8b). This initial decrease in Sr concentrations has been attributed by Baublys et al. (2019) to cation exchange. However, this hypothesis does not explain the Cl trends. As such ultrafiltration could be one of the initial processes affecting the Cl concentrations and potentially affect the ^{36}Cl values with the clay intervals acting as a barrier to Cl. There is little known about the effects on ^{36}Cl as studies to date have only measured membrane filtration between ^{35}Cl and ^{37}C and the behaviour of the ^{36}Cl remains unknown.

In summary, the low hydraulic conductivity and horizontal hydraulic head combined with low $R^{36}Cl$ values over short flow distances indicate

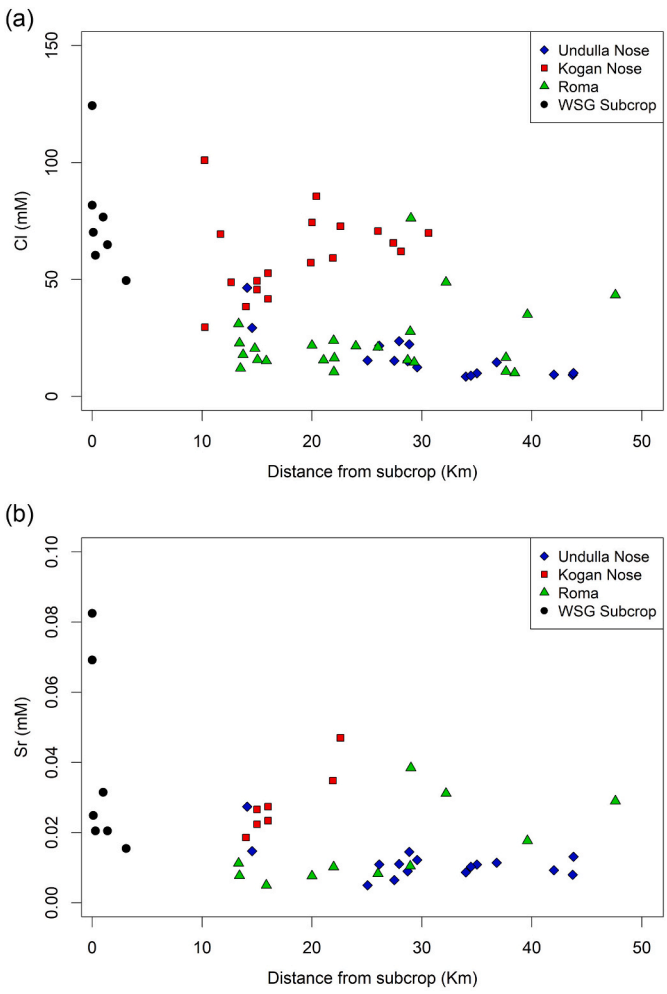

Fig. 8. Chloride and Strontium concentrations both show an initial steady decrease with distance from subcrop with Kogan Nose and Roma wells then increasing while Undulla Nose wells remain low. (a) Cl concentration vs Distance from subcrop. (b) Sr concentration vs distance from subcrop.

that the WSG groundwater has very long residence times with little to no horizontal flow. Given the ^{36}Cl values have reached secular equilibrium, it could be argued that the groundwater of the WSG overall is at near chemical equilibrium and ultrafiltration as a process must be considered. Hence, it is argued here that the combined factors above indicate a near steady chemical state and that the WSG functions as a stagnant aquitard as previously indicated by Hamilton et al. (2012). This is corroborated by the low Ca and Mg groundwater concentrations (Baublys et al., 2015, 2019) where it could be argued that the values are low as cation exchange processes have effectively reached completion.

If the WSG is functioning as a stagnant aquitard, then the question arises what other processes in addition to ultrafiltration are likely occurring. Whether the WSG is subject to either ultrafiltration or matrix diffusion, it is evident that the trends in the hydrochemical data across the WSG indicate that the groundwater composition is additionally influenced by factors other than simply distance, depth, microbial consortia and associated mineral-water interaction. This is emphasised by the trends of the $\delta^{18}O$ and Cl across the subgroup. Of note is that these hydrochemical trends are mostly visible proximal to the subcrop. Understanding the possible sources, sinks and processes that likely influence Cl concentrations is necessary to constrain interpretations on the geochemical evolution of the groundwaters.

5.3. Chloride sources and sinks

As mentioned above, previous studies (Baublys et al., 2015; Draper and Boreham, 2006; Hamilton et al., 2014b) have demonstrated that the WSG groundwater is generally meteoric in origin with transpiration being the major factor increasing the salinity of the groundwater. The main source of chloride is likely to be from seawater aerosols contained within rainfall which have been accumulating over geologic timescales. However, Owen et al. (2015) have identified that there are additional sources of Na and Cl within the WSG. Within the WSG, the Cl is present as organic and inorganic compounds within the structure of the coal, as well as adsorbed to clays and in the pore spaces of the other lithologies (Owen et al., 2015). Chloride is present as organic-bound chlorine complexes within the coal with concentrations dependant on coal type and susceptibility to degradation (Owen et al., 2015). However, the solubility and mobility of the Cl compounds in the coal in unknown. Other sources of Cl, especially in the shallow subcrop, could come from groundwater from the Main Range volcanics and shallow alluvial aquifers in what is known as the Condamine Alluvium along the eastern basin margin (Martinez et al., 2015; Owen et al., 2015). This could be a likely explanation for the higher salinity and thus Cl levels found along the eastern margins of the Surat Basin with the greatest concentration in the Kogan Nose region.

Besides ultrafiltration, loss of Cl shown by wells proximal to the subcrop could be through absorption onto coal and some clay minerals. Both organic and inorganic forms of Cl can be adsorbed/absorbed by coal (Vassilev et al., 2000). Inorganic Cl can be bound to the coal in the water layers adsorbed onto both outer and inner coal surfaces while organically bound Cl is taken up through ion exchange linkages (Vassilev et al., 2000). As such, there is the possibility that adsorption of Cl onto coal surfaces could also be a contributing process to the initial decrease in Cl concentration both in the shallow subcrop and proximal to it.

Thus, while transpiration is likely to be the main source of Cl in the groundwater, coal itself can either act as a source or a sink for Cl depending on conditions and it is the different combinations and abundance of clays, coal and methanogens that are likely to be a major influence on Cl concentrations and trends within the WSG. This requires further investigation.

5.4. Trends in $\delta^{18}O$ and chloride concentrations across the WSG

There are three distinct patterns evident in the $\delta^{18}O$ data across the WSG with distance as well as trends with the Cl concentrations. Wells within and immediately adjacent to the subcrop show decreasing $\delta^{18}O$ values and Cl concentrations with increasing distance from subcrop (Black circles in Figs. 9 and 10). All three production regions then show the opposite trend in Cl concentrations with Cl concentrations increasing with a decrease in $\delta^{18}O$ values (Fig. 9), apart from three Kogan Nose wells. These three wells have the same, more positive $\delta^{18}O$ values and higher Cl concentrations, similar to the groundwater of the subcrop wells. All three wells are shallow with two of them only screened in the Juandah rather than both the Juandah and underlying Taroom coal measures.

The $\delta^{18}O$ values for each of the production regions show three different trends with distance; the Kogan Nose $\delta^{18}O$ values become more negative with distance, and the Roma are relatively constant with a degree of scatter (the three Roma wells with the most negative $\delta^{18}O$ are the ones distant from the Hutton-Wallumbilla Fault). The Undulla Nose $\delta^{18}O$ values show the opposite trend and become more positive with distance (Fig. 10).

The shift to more negative $\delta^{18}O$ values with increasing distance from subcrop is expected and is indicative of older groundwater from recharge during a colder, wetter climate. This is demonstrated in both the Kogan Nose (except for the 3 shallow wells), Roma production regions and the WSG wells proximal to the subcrop. The opposite holds for the Undulla Nose wells where the most negative $\delta^{18}O$ values are found in the wells closest to the subcrop (Figs. 10 and 11). Here, $\delta^{18}O$ values then start to become more positive as distance from subcrop increases. At flow distances of ~40 km from subcrop, the $\delta^{18}O$ values of the Roma and Undulla Nose wells are essentially the same (Figs. 10 and 11).

Particularly evident in the Undulla Nose region, the static $R^{36}Cl$ values contrast with the variation in the Cl concentrations and $\delta^{18}O$ values over groundwater flow distances of some 45 km, and likely demonstrate that there are other forces influencing groundwater composition.

Ultrafiltration does not fully explain the trends seen in the $\delta^{18}O$ with increasing distance from the subcrop (Figs. 10 and 11), nor the trends with Cl and Sr concentrations (Fig. 8). The change in $\delta^{18}O$ values from recent rainfall values and those values found in the shallow subcrop to the more negative values found deeper in the WSG were expected and reflect colder and/or wetter past climate conditions during recharge. However, the subsequent increase in the Undulla Nose $\delta^{18}O$ values with increasing distance requires explanation (Fig. 10). Two possible explanations for these trends are:

1) Groundwater flow in the Undulla Nose is towards the subcrop and not into the deeper basin; and/or
2) Fluid-rock interactions are gradually fractionating the $\delta^{18}O$ in the groundwater.

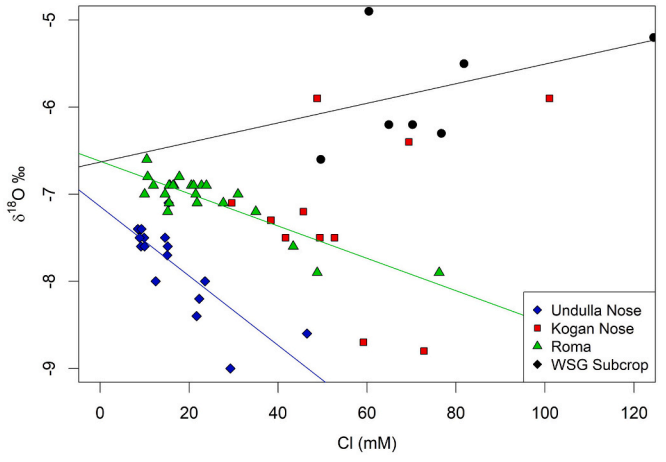

Fig. 9. Groundwater chloride and $\delta^{18}O$ trends across the WSG subcrop and production regions with associated trendlines.

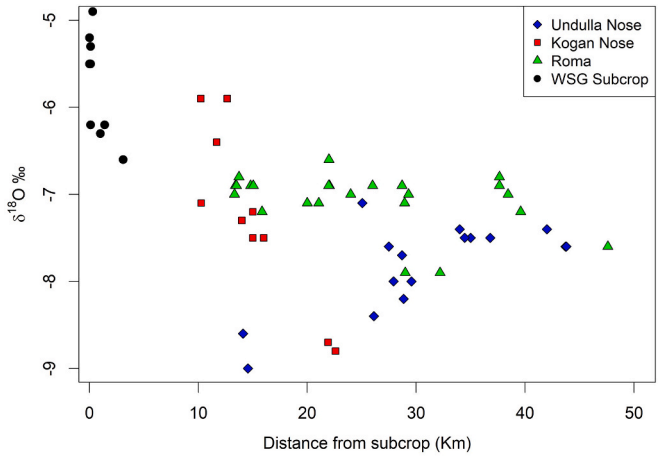

Fig. 10. Co-produced groundwater for each of the three production regions exhibit distinctive trends in $\delta^{18}O$ data as flow distance increases from subcrop.

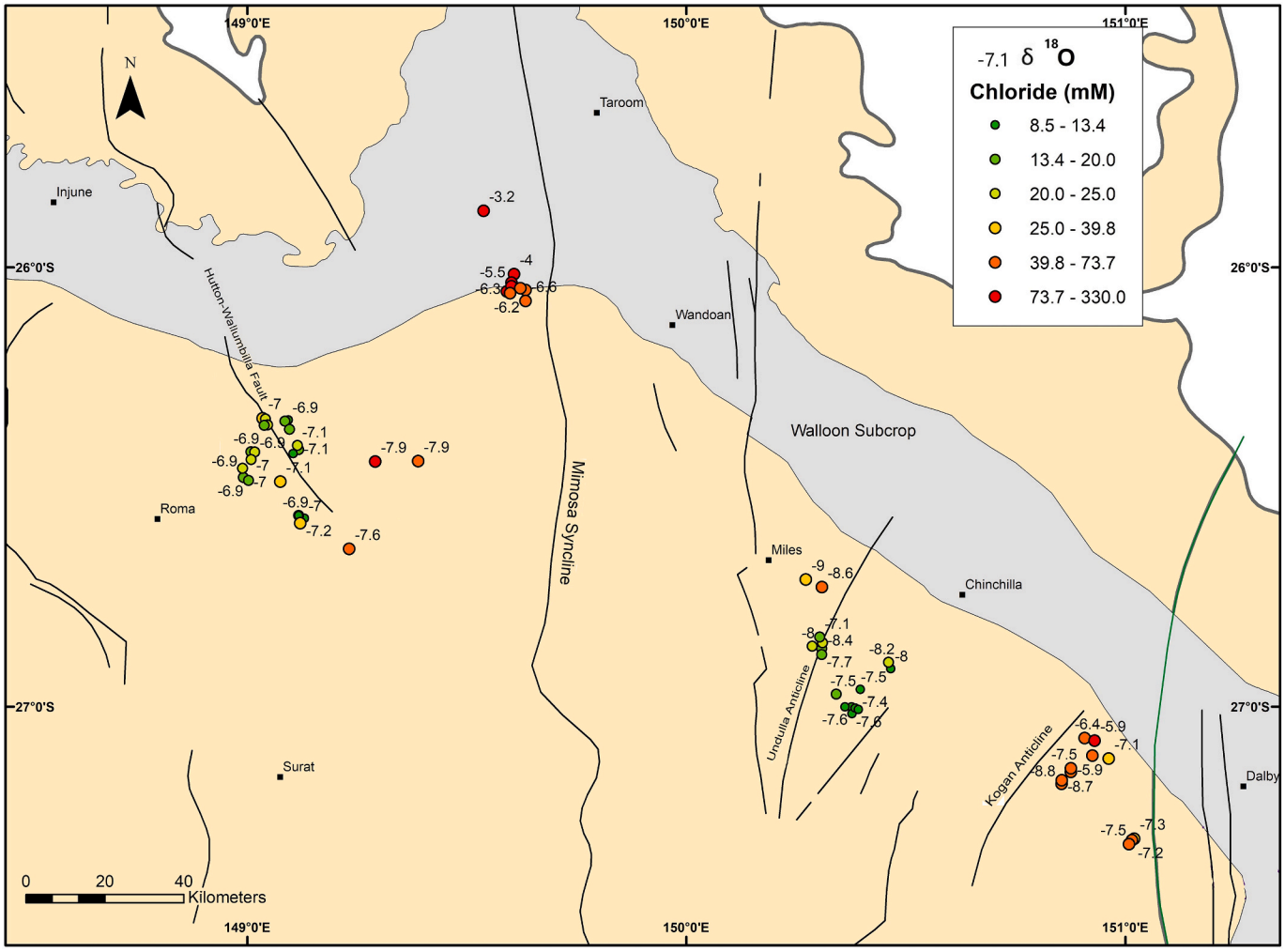

Fig. 11. Map of co-produced groundwater $\delta^{18}O$ values for the three production regions plus wells in and adjacent to the subcrop. The coloured circles indicate Cl concentration while the numbers are the $\delta^{18}O$ values.

The Undulla Nose region is an area of very low horizontal hydraulic pressure gradient (Fig. 6), no real variation in $R^{36}Cl$ values and TDS values that do not increase with distance unlike the Roma and Kogan Nose regions. There are trends in the $\delta^{18}O$ and the Cl concentrations with distance, which are the reverse of those shown in the Roma and Kogan Nose regions and could be simply explained by a reverse flow in an area known to have very low hydraulic head gradient.

Low-temperature fluid-rock interactions can also cause fractionation of isotopes such as $^{18}O/^{16}O$ and $^{87}Sr/^{86}Sr$ (Clark and Fritz, 1999) but do not affect Cl concentrations, as the minerals that are involved in these reactions generally do not contain Cl. Cation exchange with montmorillonite combined with plagioclase weathering are processes occurring in the WSG (Baublys et al., 2019). These processes may cause the initial drop in Sr concentrations with the subsequent weathering of plagioclase being responsible for an overall decrease in the radiogenic Sr found in the groundwater. This is a possible explanation of the trends seen in the geochemical data that are most dominant within the first 10–15 km of the subcrop. As such, it is likely that one process influencing the $\delta^{18}O$ values, apart from different recharge conditions, is low temperature water-rock interactions, whereby a fractionation occurs during hydration in the weathering reaction of feldspar to clay. However, oxygen and hydrogen are generally affected in opposite directions resulting in ^{2}H-enriched and ^{18}O-depleted groundwater by hydration of primary silicates during the weathering process (Clark and Fritz, 1999). Plagioclase is the dominant mineral in the subgroup ranging from 17% - 47% but clays are also present (Baublys et al., 2019). Most of the $\delta^{18}O$ and $\delta^{2}H$ values fall above the meteoric water line which supports the argument that the weathering reactions are likely to contribute to the isotopic shift; however, a trend towards depleted $\delta^{18}O$ values with distance from recharge and progressive water-rock reactions towards the centre of the basin would be expected. As $\delta^{18}O$ values only decrease with distance in the Kogan Nose area, it is unlikely that this process is dominating the shift in $\delta^{18}O$. It is more likely that the groundwater around the Undulla Nose is flowing towards the subcrop rather than towards the centre of the Surat Basin. The existing hydraulic head distribution in the area is scarce but generally indicates very low gradients and flow inversion towards the subcrop is possible. This phenomenon was demonstrated for other hydrological units, e.g., the Hutton Sandstone, in the Surat Basin where groundwater flows towards the east, rather than as historically believed to the west (OGIA, 2016; Ransley et al., 2015; Suckow et al., 2020; Vink et al., 2020).

6. Summary and Conclusions

Basin wide, the Walloon Subgroup functions as a stagnant aquitard as indicated by the loss of cosmogenic tracers (^{14}C, ^{36}Cl) and the shift in $\delta^{18}O$ to more negative values indicating that groundwater is old with very low horizontal groundwater flow. Consequently, it can be assumed that the accumulated methane is similarly old, and reinjection of methanogens occurred much earlier than the 50,000 years hypothesized

in Baublys et al. (2015). Low temperature reactions dominate such as adsorption, cation exchange and silicate weathering along with diffusive processes such as minor ultrafiltration and matrix diffusion which need to be considered.

These low temperature reactions such as cation exchange and diffusive processes such as ultrafiltration are the main drivers for solute retention as indicated by decrease in Sr and Cl concentrations over short groundwater flow distances (<10 km). While the Walloon Subgroup is effectively a stagnant aquitard, the trends in $\delta^{18}O$ and Cl for the Undulla Nose region require consideration that groundwater flow while minimal, is towards the subcrop rather than deeper into the central Surat Basin. Overall, the Walloon Subgroup is dominated by local fluid-rock and microbial interactions rather than larger regional scale influences. As well this study raises questions regarding the extent of recharge into the WSG.

Author statement

Baublys: concept, analyses, methodology, original draft preparation, data interpretation, editing.

Hofmann: draft preparation, data interpretation, editing.

Golding: draft preparation, data interpretation, editing.

Esterle: draft preparation, editing.

Cendon: draft preparation, editing.

Vink: draft preparation, editing.

Declaration of Competing Interest

The authors declare that they have no known competing financial interests or personal relationships that could have appeared to influence the work reported in this paper.

Acknowledgements

The authors wish to acknowledge financial and logistical support from QGC – A BG Group Business, Santos Ltd., Total SA, the Australian Research Council (LP100200730) and the Australian and Nuclear Science Technology Organisation (10168). Thank you to QGC (Queensland Gas Corporation) for the additional major ion data featured in some of the plots and Nicole Lennard for help with Fig. 2. M. Caffery (UQ) BSc Honours work on the Kogan Nose assisted in interpretations in this paper. We are grateful to the re.viewers for their time and insightful comments.

Appendix A. Supplementary data

Supplementary data to this article can be found online at https://doi.org/10.1016/j.coal.2021.103841.

References

Armstrong, S.C., Sturchio, N.C., Hendry, M.J., 1998. Strontium isotopic evidence on the chemical evolution of pore waters in the Milk River aquifer, Alberta, Canada. Appl. Geochem. 13 (4), 463–475.

Baublys, K.A., Hamilton, S.K., Golding, S.D., Vink, S., Esterle, J., 2015. Microbial controls on the origin and evolution of coal seam gases and production waters of the Walloon Subgroup; Surat Basin, Australia. Int. J. Coal Geol. 147-148, 85–104.

Baublys, K.A., Hamilton, S.K., Hofmann, H., Golding, S.D., 2019. A strontium (87Sr/86Sr) isotopic study on the chemical evolution and migration of groundwaters in a low-rank coal seam gas reservoir (Surat Basin, Australia). Appl. Geochem. 101, 1–18.

Bentley, H.W., et al., 1986. Chlorine 36 - Dating of very old groundwater 1. The Great Artesian Basin, Australia. Water Resour. Res. 22 (13), 1991–2001.

Bernard, B., Brooks, J.M., Sackett, W.M., 1977. A Geochemical Model for Characterization of Hydrocarbon Gas Sources in Marine Sediments, Offshore Technology Conference. ISBN 1555635709.

Capo, R.C., et al., 2014. The strontium isotopic evolution of Marcellus Formation produced waters, southwestern Pennsylvania. Int. J. Coal Geol. 126, 57–63.

Cartwright, I., Currell, M.J., Cendón, D.I., Meredith, K.T., 2020. A review of the use of radiocarbon to estimate groundwater residence times in semi-arid and arid areas. J. Hydrol. 580, 124247.

Clark, I.D., Fritz, P., 1999. Environmental Isotopes in Hydrogeology. CRC Press, USA, p. 327.

Cook, A.G., Draper, J.J., 2013. Surat Basin Chapter 7.5 in Jell, P.A., (ed) Geology of Queensland. Geological Survey of Queensland 533–539.

CSIRO, 2014. Aquifer Connectivity within the Great Artesian Basin, and the Surat, Bowen and Galilee Basins, Background Review. Commonweath of Australia. Australian Government. https://www.environment.gov.au/water/publications/background-review-aquifer-connectivity.

Davidson, M., Airey, P., 1982. The effect of dispersion on the establishment of a paleoclimatic record from groundwater. J. Hydrol. 58 (1–2), 131–147.

DNRME, 2019. Petroleum and gas reserves statistics (December 2019). In: Natural Resources, M.A.E (Ed.), Department of Natural Resources, Mines and Energy. Queensland Government. https://www.data.qld.gov.au/dataset/petroleum-gas-production-and-reserve-statistics/resource/351e9bd4-d9a1-4d60-a2ed-0e56cae79c4a.

Draper, J.J., Boreham, J.C., 2006. Geological controls on exploitable coal seam gas distribution in Queensland. APPEA J. 46, 674, 202 p.

Esterle, J.S., HAMILTON, S.K., WARD, V., TYSON, S., SLIWA, R., 2013. Scales of geological heterogeneity within the Walloon Subgroup and its coal measures. Report by School of Earth Sciences. University of Queensland for Queensland Department of Natural Resources and Mines, Brisbane, 50pp.

Evans, P.N., et al., 2015. Methane metabolism in the archaeal phylum Bathyarchaeota revealed by genome-centric metagenomics. Science 350 (6259), 434–438.

Exon, N.F., 1976. Geology of the Surat Basin in Queensland, 166. Australian Government Publishing Service. https://d28rz98at9flks.cloudfront.net/77/Bull_166.pdf.

Fallon, S., Fifield, L.K., Chappell, J., 2010. The next chapter in radiocarbon dating at the Australian National University: status report on the single stage AMS. Nucl. Instrum. Methods Phys. Res., Sect. B 268 (7–8), 898–901.

Fifield, L.K.J., 1999. Accelerator mass spectrometry and its applications. Rep. Prog. Phys. 62 (8), 1223.

Geological Survey of Queensland, G, 2013. Geological Survey of Queensland, 2013. Queensland Digital Exploration Reports (QDEX) System (Online). https://www.business.qld.gov.au/industries/mining-energy-water/resources/minerals-coal/online-services/gsq-open-data-portal.

Golding, S.D., Boreham, C.J., Esterle, J.S., 2013. Stable isotope geochemistry of coal bed and shale gas and related production waters: A review. International Journal of Coal Geology 120, 24–40.

Habermehl, M., 2002. Hydrogeology, Hydrochemistry and Isotope Hydrology of the Great Artesian Basin.

Habermehl, M., 2006. The Great Artesian Basin, Australia, 82. https://www.un-igrac.org/sites/default/files/resources/files/GWMATE%20Books%20-%20Non-renewable%20grounwater%20resources.pdf#page=76.

Hamilton, S.K., Esterle, J.S., Golding, S.D., 2012. Geological interpretation of gas content trends, Walloon Subgroup, eastern Surat Basin, Queensland, Australia. International Journal of Coal Geology 101, 21–35.

Hamilton, S.K., Esterle, J.S., Sliwa, R., 2014a. Stratigraphic and depositional framework of the Walloon Subgroup, eastern Surat Basin, Queensland. Aust. J. Earth Sci. 61 (8), 1061–1080.

Hamilton, S.K., Golding, S.D., Baublys, K.A., Esterle, J.S., 2014b. Stable isotopic and molecular composition of desorbed coal seam gases from the Walloon Subgroup, eastern Surat Basin, Australia. Int. J. Coal Geol. 122, 21–36.

Hart, M., Whitworth, T.M., Atekwana, E., 2008. Hyperfiltration of sodium chloride through kaolinite membranes under relatively low-heads–Implications for groundwater assessment. Appl. Geochem. 23 (6), 1691–1702.

Hodgkinson, J., Grigorescu, M., 2013. Background research for selection of potential geostorage targets-case studies from the Surat Basin, Queensland. Aust. J. Earth Sci. 60 (1), 71–89.

Hodgkinson, J., Hortle, A., McKillop, M., 2010. The application of hydrodynamic analysis in the assessment of regional aquifers for carbon geostorage: preliminary results for the Surat Basin, Queensland. APPEA J. 50 (1), 445–462.

Iverach, C.P., Beckmann, S., Cendón, D.I., Manefield, M., Kelly, B.F., 2017. Biogeochemical constraints on the origin of methane in an alluvial aquifer: evidence for the upward migration of methane from underlying coal measures. Biogeosciences 14 (1), 215–228.

Jell, P.A., 2013. Geology of Queensland. Geological Survey of Queensland. https://nla.gov.au/nla.cat-vn6155207.

Korsch, R.J., Totterdell, J.M., 2009. Subsidence history and basin phases of the Bowen, Gunnedah and Surat Basins, eastern Australia. Australian Journal of Earth Sciences 56, 335–353.

Leaney, F., Herczeg, A., Dighton, J., 1994. New developments for the direct CO2 absorption method for radiocarbon analysis. Quat. Sci. Rev. 13 (2), 171–178.

Lehmann, B.E., Davis, S.N., Fabryka-Martin, J.T., 1993. Atmospheric and subsurface sources of stable and radioactive nuclides used for groundwater dating. Water Resour. Res. 29 (7), 2027–2040.

Lehmann, B.E., et al., 2003. A comparison of groundwater dating with 81Kr, 36Cl and 4He in four wells of the Great Artesian Basin, Australia. Earth Planet. Sci. Lett. 211 (3), 237–250.

Mahara, Y., et al., 2009. Groundwater dating by estimation of groundwater flow velocity and dissolved 4He accumulation rate calibrated by 36Cl in the Great Artesian Basin, Australia. Earth Planet. Sci. Lett. 287 (1–2), 43–56.

Martin, M.A., Wakefield, M., MacPhail, M.K., Pearce, T., Edwards, H.E., 2013. Sedimentology and stratigraphy of an intra-cratonic basin coal seam gas play: Walloon Subgroup of the Surat Basin, eastern Australia. Pet. Geosci. 19 (1), 21–38.

Martinez, J.L., Raiber, M., Cox, M.E., 2015. Assessment of groundwater–surface water interaction using long-term hydrochemical data and isotope hydrology: headwaters of the Condamine River, Southeast Queensland, Australia. Sci. Total Environ. 536, 499–516.

Mathew, P., 1979. The Natural Radioactivity of Brown Coal in the Latrobe Valley and Its Application to Exploration and Grade Control in Coal Winning. Report 180. CSIRO.
McIntosh, J.C., Martini, A.M., 2008. Hydrogeochemical Indicators for Microbial Methane in Fractured Organic-Rich Shales: Case Studies of the Antrim, New Albany, and Ohio Shales.
Milkov, A.V., Etiope, G., 2018. Revised genetic diagrams for natural gases based on a global dataset of >20,000 samples. Org. Geochem. 125, 109–120.
Moore, C.R., Doherty, J., Howell, S., Erriah, L., 2015. Some challenges posed by coal bed methane regional assessment modeling. Groundwater 53 (5), 737–747.
Neuzil, C.E., Person, M., 2017. Reexamining ultrafiltration and solute transport in groundwater. Water Resour. Res. 53 (6), 4922–4941.
OGIA, 2016. Hydrogeological Conceptualisation Report for the Surat Cumulative Management Area. Department of Natural Resources and Mines, Brisbane, Australia.
OGIA, 2019. Underground Water Impact Report for the Surat Cumulative Management Area. In: Office of Groundwater Impact Assessment. Department of Natural Resources, M.a.E. (Editor). Queensland Government, Brisbane Queensland, Australia, p. 274. https://www.dnrme.qld.gov.au/_data/assets/pdf_file/0019/1461241/uwir-full-report.pdf.
Owen, D.D.R., Raiber, M., Cox, M.E., 2015. Relationships between major ions in coal seam gas groundwaters: examples from the Surat and Clarence-Moreton basins. Int. J. Coal Geol. 137, 77–91.
Phillips, F.M., 2013. Chlorine-36 dating of old groundwater. In: Isotope Methods for Dating Old Groundwater, pp. 125–152.
Phillips, F.M., Bentley, H.W., 1987. Isotopic fractionation during ion filtration: I. Theory. Geochim. Cosmochim. Acta 51 (3), 683–695.
Ransley, T., Smerdon, B., 2012. Hydrostratigraphy, hydrogeology and system conceptualisation of the Great Artesian Basin. In: A Technical Report to the Australian Government from the CSIRO Great Artesian Basin Water Resource Assessment. CSIRO Water for a Healthy Country Flagship Australia.
Ransley, T., et al., 2015. Groundwater Hydrochemical Characterisation of the Surat Region and Laura Basin-—Queensland, Applying Geoscience to Australia's Most Important Challenges-Geoscience Australia Report 2015/5.
Ryan, D.J., Hall, A., Erriah, L., Wilson, P.B., 2012. The Walloon coal seam gas play, Surat Basin, Queensland. APPEA Journal 52, 273–289.
Scheiber, L., et al., 2020. Hydrochemical apportioning of irrigation groundwater sources in an alluvial aquifer. Sci. Total Environ. 744, 140506.
Schoell, M., 1983. Genetic characterization of natural gases. AAPG Bull. 67 (12), 2225–2238.
Scott, S., Anderson, B., Crosdale, P., Dingwall, J., Leblang, G., 2004. Revised Geology and Coal Seam Gas Characteristics of the Walloon Subgroup-Surat Basin (Queensland).
Sliwa, R. and Esterle, J., 2008. Re-evaluation of structure and sedimentary packages in the eastern Surat Basin. In Editors: Blevin, J. E.; Bradshaw, B. E.; Uruski, C. Source: Petroleum Exploration Society of Australia Special Publication, EABS 2008, 525, Third eastern Australasian basins symposium; EABS III; energy security for the 21st century; symposium proceedings CD.
Smerdon, B., Ransley, T., Radke, B., Kellett, J., 2012. Water Resource Assessment for the Great Artesian Basin. In: A report to the Australian government from the CSIRO Great Artesian Basin water resource Assessment. CSIRO Water for a Healthy Country Flagship, Australia, p. 3.
Stueber, A.M., Pushkar, P., Hetherington, E.A., 1987. A strontium isotopic study of formation waters from the Illinois basin, USA. Appl. Geochem. 2 (5–6), 477–494.
Stuiver, M., Polach, H.A., 1977. Discussion reporting of 14C data. Radiocarbon 19 (3), 355–363.
Strapoc, D., et al., 2011. Biogeochemistry of Microbial Coal-Bed Methane. In: Jeanloz, R., Freeman, K.H. (Eds.), Annual Review of Earth and Planetary Sciences. Annual Review of Earth and Planetary Sciences 39, 617–656.
Suckow, A., Taylor, A., Davies, P., Leaney, F., 2016. Geochemical Baseline Monitoring. Final Report. CSIRO, Australia. https://publications.csiro.au/rpr/download?pid=csiro:EP156656&dsid=DS2.
Suckow, A., Raiber, M., Deslandes, A., Gerber, C., 2018. Constraining Conceptual Groundwater Models for the Hutton and Precipice Aquifers in the Surat Basin through Tracer Data. Final Report. CSIRO, Australian. https://gisera.csiro.au/wp-content/uploads/2018/03/Water-6-Milestone-2-Report-1.pdf.
Suckow, A., et al., 2020. Reconciling contradictory environmental tracer ages in multi-tracer studies to characterize the aquifer and quantify deep groundwater flow: an example from the Hutton Sandstone, Great Artesian Basin, Australia. Hydrogeol. J. 28 (1), 75–87.
Sudicky, E.A., Frind, E.O., 1981. C-14 Dating of groundwater in confined aquifers - Implications of aquitard diffusion. Water Resour. Res. 17 (4), 1060–1064.
Sudicky, E.A., Frind, E.O., 1982. Contaminant transport in fractured porous-media - Analytical solutions for a system of parallel fractures. Water Resour. Res. 18 (6), 1634–1642.
USQ, 2011. Preliminary Assessment of Cumulative Drawdown Impacts in the Surat Basin Associated with the Coal Seam Gas Industry. University of Southern, Queensland.
Van Voast, W.A., 2003. Geochemical signature of formation waters associated with coalbed methane. AAPG Bull. 87 (4), 667–676.
Vassilev, S.V., Eskenazy, G.M., Vassileva, C.G., 2000. Contents, modes of occurrence and origin of chlorine and bromine in coal. Fuel 79 (8), 903–921.
Vink, S., Underschultz, J., Guiton, S., Xu, J., Honari, V., 2020. Flow system of the Hutton sandstone in the northern Surat Basin, Australia. Hydrogeology Journal 28 (1), 89–102.
Whiticar, M.J., Faber, E., Schoell, M., 1986. Biogenic methane formation in the marine and fresh-water environments – CO2 reduction vs acetate fermentation isotope evidence. Geochim. Cosmochim. Acta 50 (5), 693–709.
Wilcken, K., et al., 2017. Accelerator mass spectrometry on SIRIUS: New 6 MV spectrometer at ANSTO. Nucl. Instrum. Methods Phys. Res., Sect. B 406, 278–282.
Winterle, J., 1998. Matrix Diffusion Summary Report. Prepared for the US Nuclear Regulatory Commission. Center for Nuclear Regulatory Analyses, San Antonio, Texas.